Generation of quinolone antimalarials targeting the *Plasmodium falciparum* mitochondrial respiratory chain for the treatment and prophylaxis of malaria

Giancarlo A. Biagini[a], Nicholas Fisher[a], Alison E. Shone[a], Murad A. Mubaraki[a], Abhishek Srivastava[a], Alisdair Hill[a], Thomas Antoine[a], Ashley J. Warman[a], Jill Davies[a], Chandrakala Pidathala[b], Richard K. Amewu[b], Suet C. Leung[b], Raman Sharma[b], Peter Gibbons[b], David W. Hong[b], Bénédicte Pacorel[b], Alexandre S. Lawrenson[b], Sitthivut Charoensutthivarakul[b], Lee Taylor[b], Olivier Berger[b], Alison Mbekeani[a], Paul A. Stocks[a], Gemma L. Nixon[a], James Chadwick[b], Janet Hemingway[a,1], Michael J. Delves[c], Robert E. Sinden[c], Anne-Marie Zeeman[d], Clemens H. M. Kocken[d], Neil G. Berry[b], Paul M. O'Neill[b,1], and Stephen A. Ward[a,1]

[a]Molecular and Biochemical Parasitology, Liverpool School of Tropical Medicine, University of Liverpool, Liverpool L3 5QA, United Kingdom; [b]Department of Chemistry, University of Liverpool, Liverpool L69 7ZD, United Kingdom; [c]Department of Life Sciences, Imperial College London, London SW7 2AZ, United Kingdom; and [d]Department of Parasitology, Biomedical Primate Research Centre, 2280 GH, Rijswijk, The Netherlands

Contributed by Janet Hemingway, April 17, 2012 (sent for review December 7, 2011)

There is an urgent need for new antimalarial drugs with novel mechanisms of action to deliver effective control and eradication programs. Parasite resistance to all existing antimalarial classes, including the artemisinins, has been reported during their clinical use. A failure to generate new antimalarials with novel mechanisms of action that circumvent the current resistance challenges will contribute to a resurgence in the disease which would represent a global health emergency. Here we present a unique generation of quinolone lead antimalarials with a dual mechanism of action against two respiratory enzymes, NADH:ubiquinone oxidoreductase (*Plasmodium falciparum* NDH2) and cytochrome bc_1. Inhibitor specificity for the two enzymes can be controlled subtly by manipulation of the privileged quinolone core at the 2 or 3 position. Inhibitors display potent (nanomolar) activity against both parasite enzymes and against multidrug-resistant *P. falciparum* parasites as evidenced by rapid and selective depolarization of the parasite mitochondrial membrane potential, leading to a disruption of pyrimidine metabolism and parasite death. Several analogs also display activity against liver-stage parasites (*Plasmodium cynomolgi*) as well as transmission-blocking properties. Lead optimized molecules also display potent oral antimalarial activity in the *Plasmodium berghei* mouse malaria model associated with favorable pharmacokinetic features that are aligned with a single-dose treatment. The ease and low cost of synthesis of these inhibitors fulfill the target product profile for the generation of a potent, safe, and inexpensive drug with the potential for eventual clinical deployment in the control and eradication of falciparum malaria.

The discovery of atovaquone 20 years ago validated the malaria parasite's mitochondrial electron transport chain (ETC) as an exploitable drug target. Atovaquone targets the ETC at the level of the bc_1 complex (1), with inhibition preventing proton pumping, resulting in a loss of mitochondrial membrane potential (2) and eventual organelle dysfunction, an important function of which is to provide intermediates for pyrimidine synthesis (3, 4). The bc_1 complex requires reducing equivalents provided by ubiquinol, which in turn is generated by membrane-bound dehydrogenases upstream in the ETC that catalyze redox reactions by reducing ubiquinone. The parasite lacks the canonical protonmotive NADH dehydrogenase (Complex I) but instead harbors a bacterial-like type II NADH:ubiquinone oxidoreductase, *Plasmodium falciparum* NDH2 (PfNDH2) (5). Based on these key observations, we undertook a drug-discovery initiative to develop cost-effective inhibitors capable of inhibiting PfNDH2 with the goal of providing antimalarials that overcome the limitations of the expensive atovaquone. Although our initial drug-discovery efforts were focused on optimization of activity versus PfNDH2, we found, during hit-to-lead development, that optimized structures with single-digit nanomolar activity versus the primary target also were active at the parasite bc_1 complex. This dual inhibitory effect also is seen with the starting point for this program, hydroxy-2-dodecyl-4-(1H)quinolone (HDQ), suggesting that the quinolone pharmacophore is a privileged scaffold for inhibition of both drug targets. Such multitarget drugs are seen increasingly as having therapeutic benefit over drugs acting exclusively at one site (6). Here we describe the development of PfNDH2/bc_1 dual-acting lead antimalarial compounds possessing favorable pharmacodynamic and pharmacokinetic features for the treatment and prophylaxis of uncomplicated malaria.

Results and Discussion

Generation of Hits Against PfNDH2 and bc_1. A high-throughput screen (HTS) against PfNDH2 was set up using recombinant PfNDH2 expressed in a heterologous expression system in *Escherichia coli* NADH dehydrogenase knockout strain ANN0222 (*nuoB::nptI-sacRB, ndh::tet*) (7), eliminating background NADH:quinol oxidoreductase activity. An assay protocol suitable for HTS was optimized and validated for screening with the Z' ranging from 0.66 to 0.9 and a signal-to-background ratio >10. A chemoinformatics strategy was initiated using HDQ (7), a dual inhibitor of PfNDH2 and bc_1 (but with poor pharmacokinetics and drug-like properties), as a query molecule to perform similarity and scaffold-hopping activities. A number of algorithms, including applied molecular fingerprints (8), turbo similarity (9), principal components analysis, Bayesian modeling (10), and bioisosteric replacement strategies (11), were used to select ~17,000 compounds for screening. The focused library was selected from a commercial library of ~750,000 compounds (BioFocus DPI), and compounds were predicted to possess favorable absorption, distribution, metabolism, excretion, and toxicity characteristics (12). Following a primary screen, 419 actives (>30% inhibition at 20 μM) were retested in triplicate, and from these, 150 compounds were progressed for potency determination (10-point concentration curves, 1:3 dilution). From the active compounds tested for potency, 22 compounds had IC_{50} values falling between 11–40

Author contributions: G.A.B., J.H., N.G.B., P.M.O., and S.A.W. designed research; G.A.B., N.F., A.E.S., M.A.M., A.S., A.H., T.A., A.J.W., J.D., C.P., R.K.A., S.L., R.S., P.G., D.W.H., B.P., A.S.L., S.C., L.T., O.B., A.M., P.A.S., G.L.N., J.C., M.J.D., R.E.S., A.-M.Z., C.H.M.K., and N.G.B. performed research; C.P., R.K.A., S.L., P.G., D.W.H., B.P., A.S.L., S.C., L.T., O.B., A.M., P.A.S., G.L.N., and J.C. contributed new reagents/analytic tools; G.A.B., N.F., A.E.S., M.A.M., A.S., A.J.W., R.S., R.E.S., A.-M.Z., C.H.M.K., N.G.B., P.M.O., and S.A.W. analyzed data; and G.A.B., G.L.N., N.G.B., P.M.O., and S.A.W. wrote the paper.

The authors declare no conflict of interest.

Freely available online through the PNAS open access option.

[1]To whom corresponding may be addressed. E-mail: hemingway@liverpool.ac.uk, pmoneill@liv.ac.uk, or saward@liverpool.ac.uk.

This article contains supporting information online at www.pnas.org/lookup/suppl/doi:10.1073/pnas.1205651109/-/DCSupplemental.

μM, and 24 compounds had IC_{50} values <10 μM and purity >70%. These hits were observed to occupy distinct areas of chemical space (Fig. 1 and Table S1).

Twelve distinct chemotypes were identified from the hits. Hit expansion and the evaluation of "near neighbors" confirmed the selection of the quinolone core as the main target for structure–activity relationship (SAR) development. Initial studies focused on compounds with monoaryl groups at position 2; however, it was impossible to drive activity below 500 nM against the 3D7 strain of *P. falciparum*. A progression toward the close HDQ analogs, where a longer biaryl/phenoxy biaryl replaced the metabolically vulnerable HDQ side chain, improved both antimalarial and PfNDH2 activity as demonstrated by RKA073 (Fig. 2). A further structural alteration introduced a methyl substituent at position 3. This manipulation twists the 2-aryl side chain, altering the torsion angle (presumably leading to a reduction in aggregation), and resulting in better overall solubility and greatly enhanced activity. This medicinal chemistry strategy generated more than 60 compounds, as exemplified by CK-2–68 with activity of 31 nM against the *P. falciparum* 3D7 strain and 16 nM against PfNDH2. Investigations into the level of substitution in the A-ring of the quinolone core showed that F, Cl, or H at the 7 position were optimal for 3D7, W2, and PfNDH2 activity (Fig. 2, Fig. S1, and Tables S2 and S3).

Selectivity of Inhibitors for bc_1 and PfNDH2. Several trends emerged from the analysis of the in vitro activity profiles (Table S2). Incorporation of a halogen at the 7 position increased the selectivity for PfNDH2 over that for bc_1, as best demonstrated when comparing the selectivity ratios (SRs: inhibitory activity against bc_1/inhibitory activity against PfNDH2) of CK-2–68 (SR = 31) vs. CK-2–67 (SR = 2.34) and SL-2–64 (SR = 6.4) vs. SL-2–25 (SR = 1.0). Removal of the methyl linker in the side chain also imparted greater selectivity; for example, CK-2–67 with the methylene linker has a selectivity ratio of 2.34, whereas SL-2–34 without the linker has a selectivity ratio of >38. Fig. S2 demonstrates the SAR effect seen when comparing the 2-aryl and 3-aryl series of compounds. 2-Aryl quinolones provide PfNDH2 inhibition levels of less than 20 nM, whereas the directly comparable 3-aryl quinolones have PfNDH2 inhibition levels greater than 200 nM. However, 3-aryl quinolones demonstrate high levels of bc_1 inhibition, which are not unexpected given the very close structural features of this series with the known GlaxoSmithKline pyridone bc_1 inhibitors (13).

Given the potent nanomolar inhibitory activity of Sl-2–25 against the bc_1 complex, a docking experiment was performed using the yeast bc_1 crystal structure to determine the nature of the key interactions at this target site (Fig. 2*D*). Although not identical to the parasite bc_1 complex, the yeast protein shares 40% homology, and the Q_o region is extremely well conserved between the two proteins: Yeast and *P. falciparum* cytochrome *b* show 71% sequence identity in the C-terminal region of helix C and the cd1 loop region of Q_o (20/28 residues) and 85% sequence identity in the ef loop region of Q_o (11/13 residues); the key hydrogen-bonding residues E272 and H181 (from the Rieske iron-sulfur protein) are completely conserved. Docking of SL-2–25 was performed, and results showed an average GoldScore of 53.7, consistent with this inhibitor displaying potent inhibitory activity. Inspection of the docking results shows that SL-2–25 occupies a position within the Q_o site of cytochrome *b* similar to that of stigmatellin, distal to low-potential heme. Hydrogen bonds are provided to the quinolone head group via the imidazole ring of Rieske protein residue His181 (1.6 Å), with a water-bridged hydrogen bond from the side chain of cytochrome *b* 'PEWY' (ef) loop residue Glu272 (2.5 and 2.3 Å) (Fig. S3). Within cytochrome *b*, the SL-2–25 binding site is formed from residues contained within the C-terminal region of transmembrane helix C (I122, I125), helix cd1 (I147, L150), the ef loop (L269, P271, E272, L275), and the F1–F2 linker region (F296, I299) (Fig. S3). Most interactions are hydrophobic and van der Waals in nature. The side chain of I122 is predicted to form a 58-$Å^2$ van der Waals interaction with the trifluoromethoxy moiety of SL-2–25, with significant hydrophobic interactions with the pyridinyl and quinolone groups of the inhibitor provided by the side chains of P271 and L275 (26 and 33 $Å^2$, respectively).

Pharmacodynamics of bc_1/PfNDH2 Inhibitors. From the series, CK-2–68 was used for validation of the target because of its selectivity for PfNDH2. CK-2–68 demonstrated potent activity against both native and recombinant PfNDH2, with IC_{50} inhibition values of 23 ± 5 nM and 16 ± nM, respectively. Steady-state substrate competition assays indicated that CK-2–68 competes for quinone (Q_1) and not NADH-binding sites (Fig. S4 *A* and *B*), with an inhibition constant K_i value of 2.4 nM (14). CK-2–68 displayed relatively low activity (IC_{50} 500 nM) against parasite bc_1 and no activity (IC_{50} >100 μM) against parasite dihydroorotate dehydrogenase (DHODH). As with the other members of the series, CK-2–68 displayed potent activity against multidrug-resistant parasite lines including TM902CB, an atovaquone-resistant (atovaquone IC_{50} >12 μM) Thai parasite isolate carrying the cytochrome *b* mutation Y268S (Table 1). We also generated the strain 3D7-yDHODH·GFP, a transgenic derivative of *P. falciparum* 3D7 containing yeast DHODH, through electroporation of purified pHHyDHOD-GFP plasmid (4). Transfection of malaria parasites with the yeast DHODH gene has been shown previously to confer resistance to the parasite against ETC inhibitors (4); consistent with this report, CK-2–68 showed a dramatic loss of activity against 3D7-yDHODH·GFP with an IC_{50} of 4.6 μM. (The IC_{50} for atovaquone in the transgenic 3D7-yDHODH·GFP was 5.8 μM; see Table 1). CK-2–68 prevented asexual development at the midtrophozoite stage (as does atovaquone) and demonstrated a time-to-kill profile similar to that of atovaquone (Fig. 3). Through repeated exposure (over the course of 4 mo) to sublethal concentrations of CK-2–68, we generated a *P. falciparum* (K1) line with a threefold-increased tolerance to CK-2–68 (a shift of IC_{50} from 150 nM to

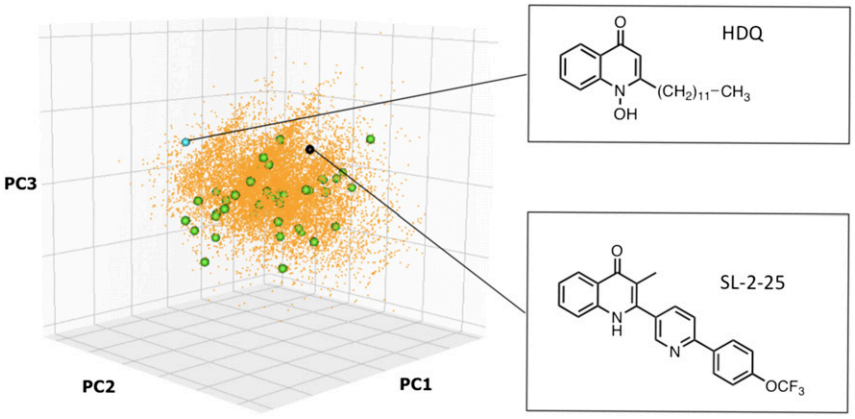

Fig. 1. 3D plot of chemical space showing progression from HDQ via hits from HTS to SL-2–25. Chemical space representation of first three principal components is based on calculated physiochemical properties of 48 hit compounds that account for 88.5% of the variance. All other compounds projected into principal component space using this model. The cyan sphere represents HDQ; orange points represent ~17,000 compounds selected via chemoinformatics methods and screened in HTS; green spheres represent 48 hits from HTS; and the back sphere represents SL-2–25. The three-component principal components analysis model was built using Knime (http://www.knime.org), and the 3D plot was produced using R using the Ruby Graph Library (http://cran.r-project.org).

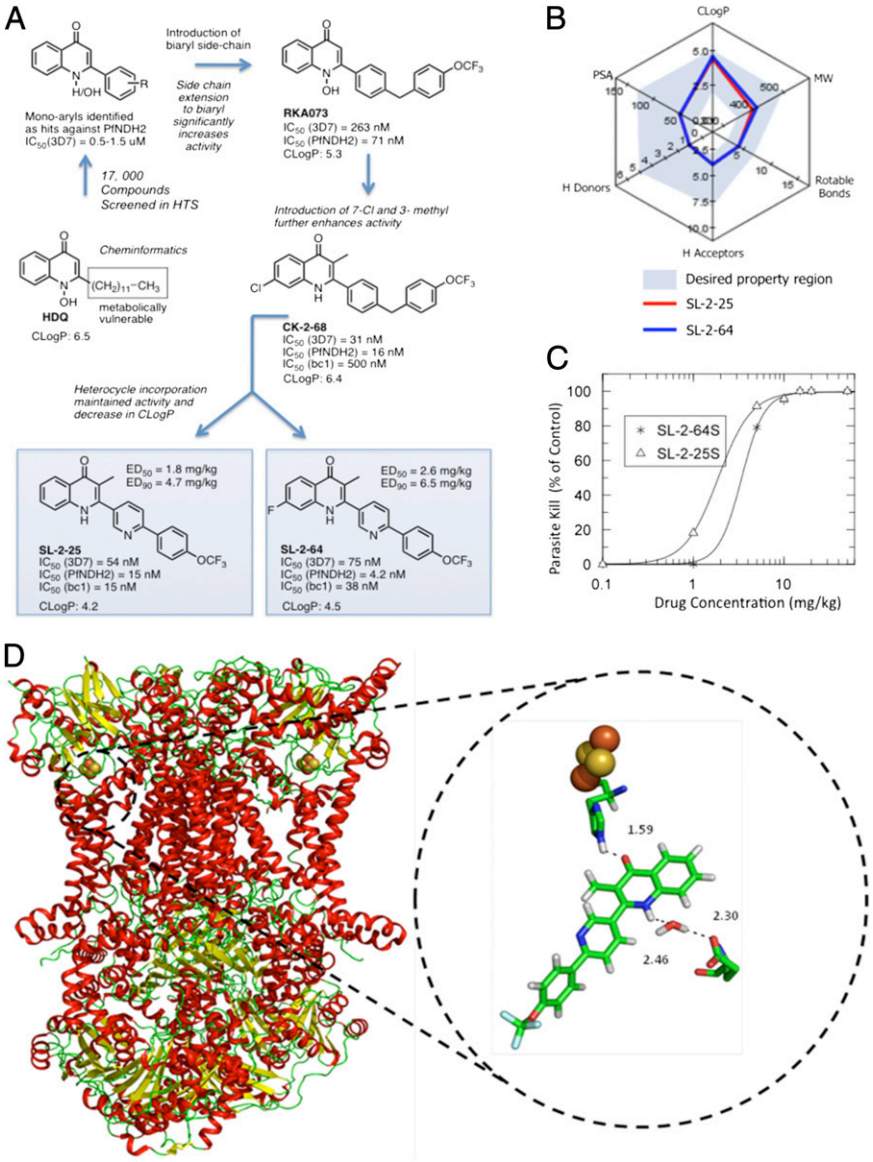

Fig. 2. (*A*) Medicinal chemistry strategy deployed in the discovery of SL-2–25 and SL-2–64. (*B*) Radar plot of physicochemical properties of SL-2–25 (red line) and SL-2–64 (blue line) and how these properties map onto the desired target (Lipinski-like) region. (*C*) Dose–response curve for lead quinolones versus *P. berghei* (four doses). (*D*) Cartoon representation of bc_1 complex with enlarged view of compound SL-2–25 docked in the Q_o site of yeast bc_1 (PDB code 3CX5). In the close-up view residues His181 (iron-sulfur protein), Glu272 (cytochrome *b*), and H-bond interactions are highlighted. Q_o site water molecule 7187 forms an H-bond bridge between Glu272 and the quinolone NH. Also shown in orange and yellow sphere representation is the Fe_2S_2 cluster (iron-sulfur protein). Interatomic distances for hydrogen-bonding interactions are given in Å.

450 nM). Subsequent analysis of the PfNDH2 gene (PFI0735c) in this strain revealed a nonsynonymous nucleotide substitution at G609A replacing isoleucine with valine at residue 203. In the absence of an atomic structure for PfNDH2, it is not possible at this stage to determine the significance of the V203I mutation; however, there are no native single-nucleotide polymorphisms in plasmodial PfNDH2 (PlasmoDB.org).

We have shown previously that, although PfNDH2 is not directly involved in proton pumping (5), inhibition of this enzyme leads to a depolarization of the mitochondrial membrane potential by virtue of starving the bc_1 of reducing equivalents (15). We therefore perfused trophozoite-stage parasites with CK-2–68 and, using dynamic single-cell measurements of parasite mitochondrial membrane potential (15, 16), demonstrated rapid depolarization at concentrations as low as 1 nM, 500-fold below the IC_{50} against bc_1 (Fig. 4*A*). The mitochondrion of asexual parasites has been shown previously to provide orotate for pyrimidine biosynthesis through the activity of DHODH (3, 17). The link between mitochondrial function and pyrimidine biosynthesis was supported further by the generation of an atovaquone-resistant phenotype in transgenic *P. falciparum* parasites expressing Coenzyme Q-independent yeast DHODH (4). To confirm disruption of pyrimidine biosynthesis by CK-2–68, we undertook a targeted metabolomics approach in which we simultaneously monitored the response of 35 key parasite metabolites to CK-2–68 and atovaquone in both 3D7 and transgenic 3D7-yDHODH·GFP falciparum parasites. The metabolome dynamics following drug exposure confirms previous reports that atovaquone disrupts pyrimidine metabolism at the point of DHODH as indicated by the accumulation of dihydroorotate and reduction of downstream intermediates (Fig. 4 *B* and *C* and Fig. S4*C*). Significantly, no change in pyrimidine metabolite dynamics was observed upon atovaquone addition in the transgenic 3D7-yDHODH·GFP strain, confirming the hypothesis that in this strain the yeast DHODH rescues the parasite from bc_1-mediated inhibition of pyrimidine biosynthesis (4). CK-2–68 also was shown to disrupt pyrimidine biosynthesis, causing an increase in dihydroorotate and carbamoyl-L-aspartate indicative of a similar choke point at DHODH (Fig. 4 *B* and *C*). These data are consistent with CK-2–68 causing parasite death by inhibiting pyrimidine biosynthesis caused by the collapse of mitochondrial function. (A schematic of the ETC of *P. falciparum* is given in Fig. S5.)

As described, CK-2–68 was used as a proof-of-concept inhibitor. More drug-like leads displayed equipotent PfNDH2 and bc_1 inhibitory activity (Table 1 and Table S1), and these leads were tested further to determine their inhibitory activity against the liver and sexual stage of the parasites. Using a high-content imaging

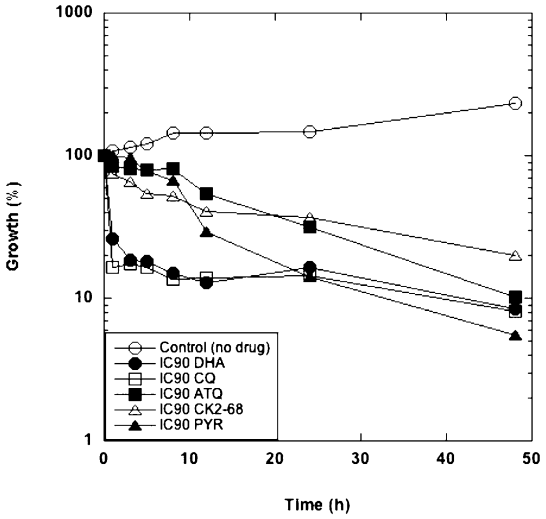

Fig. 3. Kill-rate profile of CK-2–68 (△), atovaquone (■), pyrimethamine (▲), chloroquine (□), and dihydroartemisinin (●) relative to drug-free control (○). All drugs were administered at IC_{90} concentrations.

assay, the development of liver-stage *Plasmodium cynomolgi* parasites was monitored in the presence of lead compounds (Fig. 5*A*). *P. cynomolgi*, like its close relative *Plasmodium vivax*, forms dormant liver stages as well as immediately developing liver stages, described as "small" forms (hypnozoites) and "large" forms (schizonts), respectively, in 6-d-old in vitro liver-stage cultures (18). As expected, liver-stage development of *P. cynomolgi* schizonts and hypnozoites was inhibited by incubation with the positive control primaquine. Incubation with SL-2–99 (a morpholine prodrug of SL-2-25), SL-2–25, and CK-2–68 resulted in the arrest of liver-stage *P. cynomolgi* schizont development at pharmacologically relevant exposure concentrations (see below). Schizont development is arrested early in this assay, because schizonts remain small (or disappear from culture as total parasitemia goes down with higher levels of compound) and thus are counted as hypnozoites. Hypnozoites themselves appear unaffected by these compounds, similar to previous reports with atovaquone (18).

Lead compounds also were tested for activity against sexual stages of *Plasmodium*. Neither inhibitor showed any activity against late stages IV and V (as is also the case with atovaquone). CK-2–68 displayed moderate inhibition of *P. falciparum* microgametocyte exflagellation (IC_{50} ~10 μM) similar to that seen with atovaquone (IC_{50} ~1 μM). Both CK-2–68 and SL-2–25 also showed potent activity against *Plasmodium berghei* ookinete production (IC_{50} 73 and 154 nM, respectively) (Fig. 5*B*).

In vivo experiments using *P. berghei*-infected mice demonstrated that CK-2–68 when given orally at 20 mg/kg [using 5% (vol/vol) DMSO, 5% (vol/vol) ethanol in tetraglycol as vehicle] resulted in complete parasite clearance in the Peters' standard 4-d suppressive test (19), Despite this finding, it was apparent that the partition coefficient (ClogP) needed to be reduced, and aqueous solubility needed to be enhanced to deliver a molecule with improved drug-like properties. Introduction of various heterocycles into the quinolone side chain led to the selection of a series of compounds containing a pyridine group within the side chain. Incorporation of a pyridine group reduces ClogP, improves aqueous solubility, and allows the possibility of salt formation because of the presence of the basic nitrogen (pK_a = 4.7). From more than 50 compounds SL-2–25 and SL-2–64 were selected as leads for further preclinical investigation in the murine model of malaria (Fig. 2).

Formulation of SL-2–25 (with in vitro activity of 54 nM against 3D7 and 14 nM against PfNDH2) provided the phosphate salt with ED_{50}/ED_{90} values of 1.87/4.72 mg/kg and a morpholine prodrug (Fig. S6) with ED_{50}/ED_{90} values of 10.4/15.2 mg/kg. Introduction of a fluorine at the 7 position gave SL-2–64 with comparable in vitro activity and ED_{50}/ED_{90} values of 3.3/6.48

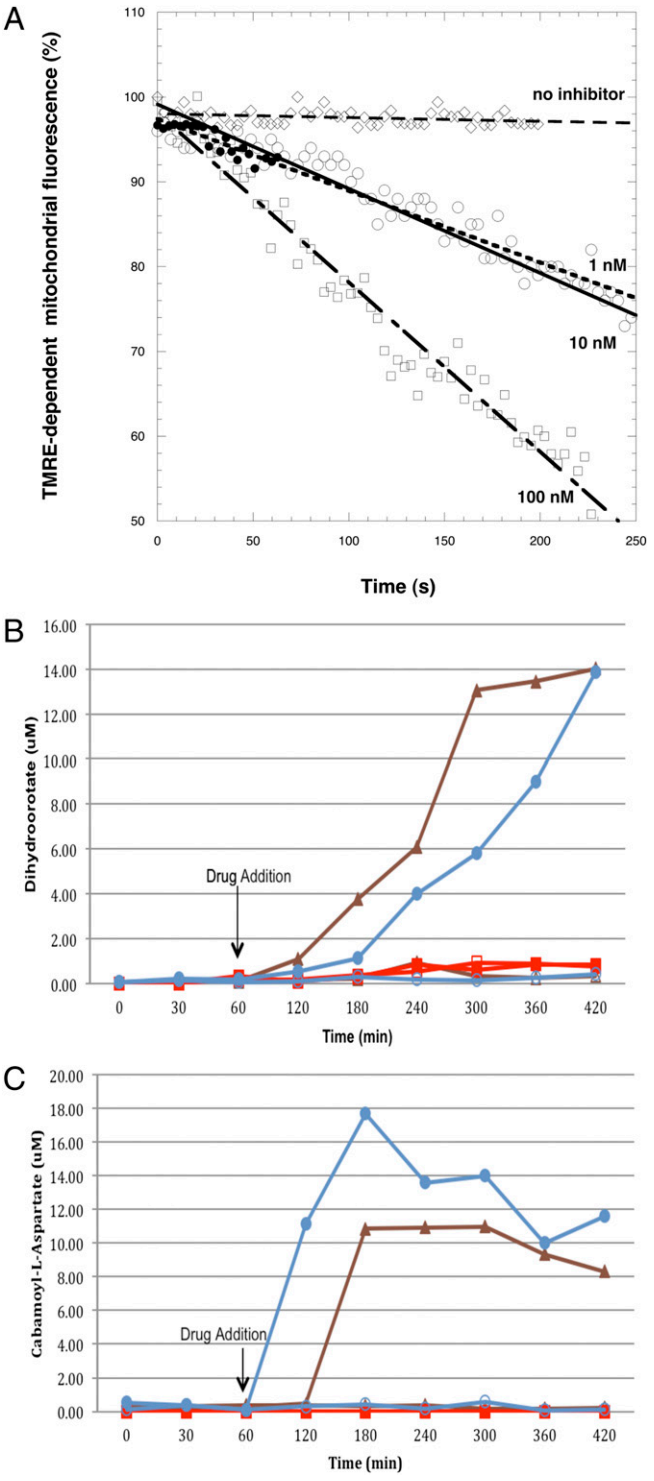

Fig. 4. (*A*) Time course of tetramethylrhodamine ethyl ester-dependent mitochondrial fluorescence after the addition of CK-2–68 to *P. falciparum*-infected erythrocytes. Data were normalized to 100% in untreated cells and to 0% in cells treated with 10 μM carbonyl cyanide m-chlorophenyl hydrazone. ◇, Untreated cells; ○, 1 nM CK-2–68; ●, 10 nM CK-2–68; □, 100 nM CK-2–68. Graph shows data derived from experiments performed independently ($n \geq 3$). (*B*) Dihydroorotate and (*C*) carbamoyl-L-aspartate concentrations in *P. falciparum* 3D7 and 3D7-yDHODH·GFP parasites following addition of 100 nM CK-26–8 and atovaquone. △, untreated 3D7 parasites; ▲, atovaquone-treated 3D7 parasites; □, untreated 3D7-yDHODH·GFP parasites; ■, atovaquone-treated 3D7-yDHODH·GFP parasites; ○, untreated 3D7 parasites; ●, CK-2–68–treated 3D7 parasites.

PHARMACOLOGY

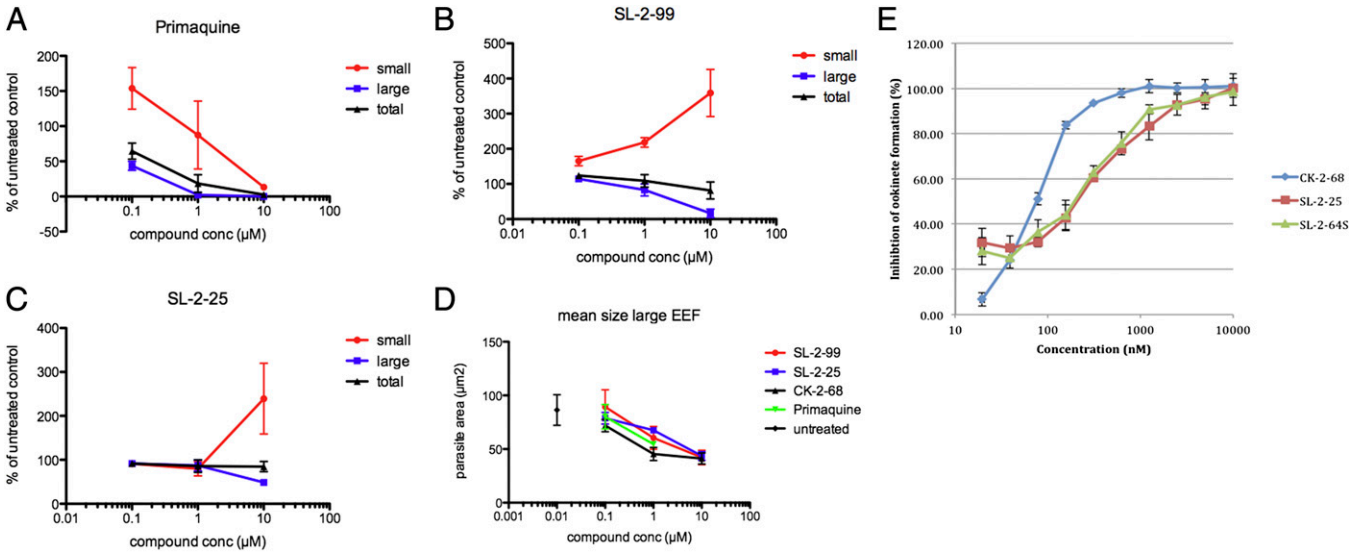

Fig. 5. Activity of lead compounds against *Plasmodium* liver (also known as exoerythrocytic forms) and sexual stages. (*A–D*) Activity of lead compounds against *P. cynomolgi* large (liver schizonts) and small (hypnozoites) forms. (*E*) Activity of lead compounds against *P. berghei* ookinete formation.

mg/kg (Fig. 2). Against the same strain, chloroquine had an ED_{50}/ED_{90} of 3.3 mg/kg/4.6 mg/kg, and artemether was active (ED_{50}/ED_{90} of 3.1 mg/kg/5.8 mg/kg), indicating that these molecules have potency similar to that of other clinically used antimalarials in this model. All compounds are synthesized in four to six high-yielding steps from inexpensive, commercially available starting materials (Figs. S1 and S6).

The pharmacokinetic features of SL-2–25 phosphate salt (5 mg/kg) were favorable following oral administration [maximum concentration, 3.1 μg/mL; time to reach maximum plasma drug concentration, 7.0 h; elimination half-life, 10.6 h; volume of distribution, 1,261.4 mL/kg; area under the curve from time zero to time t (AUC_{0-t}). 57.9 μg/h/mL; and a total body clearance of 82.1 $mL{\cdot}h^{-1}{\cdot}kg^{-1}$] (Fig. S7). These pharmacokinetic parameters are consistent with a target product profile of once-daily oral dosing for 3 d. However, an elimination half-life of 10.6 h in the mouse suggests the possibility of a single-dose cure with these molecules.

Previous antimalarial projects that have focused on the development of bc_1 inhibitors have had to be terminated because of safety concerns regarding cardiotoxicity (20). Therefore we established a beef-heart bc_1 counterscreen to assess possible mitochondrial toxicity. We have shown in the past that this screen is a better model than rodent screens to assess toxicity (16). As shown in Table 1, all lead compounds display favorable in vitro therapeutic indices relative to our comparator drug atovaquone.

In summary, we have generated potent inhibitors that are active against blood stages of *P. falciparum* malaria that have the capacity to inhibit two key enzymes in the respiratory pathway of *P. falciparum*. The use of a privileged scaffold with multitarget pharmacology, as developed here, should be an advantage both in potency across a wide range of malaria parasite strains and in protection against the rapid evolution of resistance. Initial in vivo studies confirm these inhibitors as drug-like, with properties consistent with a potential deployment role in malaria control and eradication. Further lead optimization studies are in progress to identify the most promising candidate molecules for full preclinical evaluation en route to Phase 1 clinical trials in humans.

Materials and Methods

Parasites, Culture, and Drug-Sensitivity Testing. Drug-sensitivity phenotypes of *P. falciparum* strains 3D7, K1, and TM902CB have been described previously (21, 22). *Plasmodium* blood-stage cultures were maintained by the method of Trager and Jensen (23). Growth proliferation was determined by the SYBR Green method (24). Time-to-kill curves for antimalarials were conducted by incubating parasites with drugs for variable time intervals followed by three washes in complete culture medium and a return to standard growth conditions. All values are relative to untreated controls. The transgenic 3D7-yDHOD·GFP strain was generated through electroporation of purified pHHyDHOD-GFP plasmid into ring stages of *P. falciparum* using a Bio-Rad GenePulser following the method in ref. 4.

P. cynomolgi M strain was used for in vitro liver-stage drug assays. Liver-stage drug assays were performed in primary rhesus monkey hepatocytes as described (18), with the modification of the inclusion of a 6-d drug exposure. Read out of the assay was performed using a high-content imaging system (Operetta, Perkin Elmer) analyzed with Harmony software (Perkin Elmer). Small forms (hypnozoites) were defined as having a maximum parasite area of 30 μm^2.

P. falciparum exflagellation and *P. berghei* ookinete formation were performed as described in ref. 25.

HTS. PfNDH2 activity was measured using an end-point assay in a 384-well plate format. Final assay concentrations used were 20 mM Hepes (VWR) (free acid) in dH_2O (pH 7.4), 200 μM NADH (Sigma), 10 mM KCN (Sigma), 1 μg/mL F571 membrane 10, 20 μM coenzyme Q (Q1) (C7956; Sigma). A pre-read at 340 nm was

Table 1. Enzyme and parasite inhibition profiles of electron transport chain inhibitors

Compound	3D7 IC50 (nM)	TM902CB IC_{50} (nM)	Pailin isolate P036 IC_{50} (nM)	3D7-yDHODH·GFP IC_{50} (nM)	PfNDH2 enzyme inhibition IC_{50} (nM)	Parasite bc_1 IC_{50} (nM)	Bovine heart bc_1 IC_{50} (nM)	Viability of hepG2 cells at 50 μM inhibitor (%)
Atovaquone	0.9 ± 0.01	$12 \times 10^3 \pm 1.6 \times 10^3$	0.7 ± 0.03	$5.8 \times 10^3 \pm 2.2 \times 10^3$	$>10 \times 10^3$	2 ± 1	83 ± 9	85
Chloroquine	11 ± 2	70 ± 9	51 ± 5	6 ± 2	ND	ND	ND	ND
CK-2–68	31 ± 3	184 ± 16	46 ± 21	$1.6 \times 10^3 \pm 0.2 \times 10^3$	16 ± 2	500 ± 122	465 ± 27	72
SL-2–25	54 ± 6	156 ± 22	151 ± 32	$2.2 \times 10^3 \pm 0.4 \times 10^3$	14 ± 1	15.1 ± 2.9	890 ± 151	67
SL-2–64	75 ± 9	183 ± 22	146 ± 15	$4.6 \times 10^3 \pm 0.4 \times 10^3$	4.7 ± 0.3	26.8 ± 5.6	175 ± 60	88

Data are mean from experiments performed independently ($n \geq 3$). ND, not determined.

obtained before the addition of Q1 to initiate the reaction followed by a post-read at 1 min. HDQ was used as positive control at 5 μM. The agreed quality control pass criteria were $Z' > 0.6$ and signal/background > 10. Compounds were selected by the described chemoinformatics algorithms from the BioFocus DPI compound library (Galapagos Company), and assays were performed using Pipeline Pilot (http://accelrys.com/products/pipeline-pilot) and PowerMV (11).

Molecular Docking. GOLD 5.0.1 (CCDC Software Limited 2005–2010, http://www.ccdc.cam.ac.uk/products) was used to dock SL-2–25 into the Q_o site of yeast bc_1 [Protein Data Bank (PDB) code 3CX5 (26)]. The native ligand stigmatellin was removed, and the binding site was defined as all atoms within 6 Å of the crystallographic ligand. Protons were added, and all crystallographic water molecules were removed, except for HOH7187, which has been described previously as key to the hydrogen bonding network. Constraints were applied such that docking poses were optimized for the His181 and Glu272 hydrogen bond interactions with SL-2–25. HOH7187 was allowed to spin and translate from its original position with a radius of 2 Å. The docking was performed using standard parameters except that it was repeated 25 times and gave an average GoldScore of 53.7.

Biochemistry. *P. falciparum* cell-free extracts were prepared from erythrocyte-freed parasites as described previously (16), and recombinant PfNDH2 was prepared from the *E. coli* heterologous expression strain F571 as described in ref. 7. PfNDH2 and bc_1 activities were measured as described previously (7, 16). Real-time single-cell measurements of mitochondrial membrane potential (Ψm) were performed as described previously (15, 16). Metabolite analysis of trophozoite-stage *P. falciparum* strains following drug treatment with atovaquone (2.5 nM) or CK-2–68 (50 nM) was carried based on the method of Rabinowitz and Kimball (27).

Generation of CK-2–68–Resistant *P. falciparum* and Sequencing of the PfNDH2 Gene. *P. falciparum* K1 strain was incubated for 2 d with an IC_{90} concentration of CK-2–68, followed by withdraw of the drug for 5 d. The procedure was repeated for several cycles until parasites became threefold resistant compared with wild type. The PfNDH2 gene of the CK-2–68 resistant strain was amplified from genomic DNA. Further details are given in *SI Materials and Methods*.

Metabolite Analysis in Drug-Treated Parasites. *P. falciparum* strains 3D7 and 3D7-yDHOD·GFP were maintained in synchronous cultures in a 2% hematocrit as described. Enriched trophozoite-stage parasites were generated using a VarioMACS separation unit (Miltenyi Biotec). The enriched trophozoite-stage parasites were incubated with RPMI medium 1640 (Sigma) (R8758, glutamine, and $NaHCO_3$) supplemented with 0.25% ALBUMAX II (Invitrogen), 25 mM Hepes (pH 7.4) (VWR), 40 μM hypoxanthine (Sigma), and 20 μM gentamicin sulfate (Sigma) at 37 °C under 3% O_2/4% CO_2 in N_2. At predetermined time intervals, parasite samples ($\sim 1 \times 10^8$ parasites/mL) were removed and metabolically quenched by plunging into five volumes of extraction solvent (40:40:20 acetonitrile:methanol:water solvent). No-drug controls contained a DMSO concentration equivalent to that of CK-2–68. Chromatographic separation and detection and analysis of metabolites were performed using liquid chromatography coupled to tandem mass spectrometry (LC-MS/MS). Further details are given in *SI Materials and Methods*.

Pharmacology. In vivo efficacy studies were measured against *P. berghei* NS in a standard 4-d test (19). In vivo tests were performed under UK Home Office Animals (Scientific Procedures) Act 1986. Male CD-1 mice (30 g) (Charles River) were kept in specific pathogen-free conditions and fed ad libitum. For oral administration, compounds were dissolved in standard suspending formula (0.5% sodium carboxymethylcellulose, 0.5% benzyl alcohol, 0.4% Tween 80, and 0.9% NaCl; all reagents purchased from Sigma). Mice were infected by i.p. injection with 4×10^6 infected red cells (day 0), randomized, and divided into groups of five mice for each dose. Oral treatment started 1–2 h after infection and was administered once each day for up to 3 d postinfection. Parasitemias were determined by microscopic examination of Giemsa-stained blood films taken on day 4. Pharmacokinetic studies were based on previously described methods (28). All in vivo studies were approved by the appropriate institutional animal care and use committee and were conducted in accordance with the International Conference on Harmonization safety guidelines.

ACKNOWLEDGMENTS. We thank Prof. Dennis Kyle (University of South Florida, Tampa, FL) for supplying TM90C2B; Prof. Mathirut Mungthin (Phramongkutklao College of Medicine) for the generous gift of the Pailin strain; Prof. Akhil Vaidya (Drexel University College of Medicine) for supplying purified pHHyDHOD–GFP plasmid; Prof. Thorsten Friedrich (Albert-Ludwigs-Universität) for providing *E. coli* strain ANN0222; Prof. Dominique Mazier (Pierre and Marie Curie University/Institut National de la Santé et de la Recherche Médicale) for sharing *Plasmodium* liver-stage culture technology; Alex Van Den Berg, Els Klooster, and Sandra van Amsterdam for expert technical assistance; and. the staff and patients of Ward 7Y and the Gastroenterology Unit, Royal Liverpool Hospital, for their generous donation of blood. The liver-stage work was supported by Medicines for Malaria Venture and by Wellcome Trust Grant WT078285. This work was supported by grants from the Wellcome Trust Seeding Drug Discovery Initiative, the Leverhulme Trust, and the National Institute of Health Research. M.A.M was granted a doctoral scholarship from King Saud University.

1. Fry M, Pudney M (1992) Site of action of the antimalarial hydroxynaphthoquinone, 2-[trans-4-(4′-chlorophenyl) cyclohexyl]-3-hydroxy-1,4-naphthoquinone (566C80). *Biochem Pharmacol* 43:1545–1553.
2. Srivastava IK, Rottenberg H, Vaidya AB (1997) Atovaquone, a broad spectrum antiparasitic drug, collapses mitochondrial membrane potential in a malarial parasite. *J Biol Chem* 272:3961–3966.
3. Hammond DJ, Burchell JR, Pudney M (1985) Inhibition of pyrimidine biosynthesis de novo in *Plasmodium falciparum* by 2-(4-t-butylcyclohexyl)-3-hydroxy-1,4-naphthoquinone in vitro. *Mol Biochem Parasitol* 14:97–109.
4. Painter HJ, Morrisey JM, Mather MW, Vaidya AB (2007) Specific role of mitochondrial electron transport in blood-stage *Plasmodium falciparum*. *Nature* 446:88–91.
5. Fisher N, Bray PG, Ward SA, Biagini GA (2007) The malaria parasite type II NADH: quinone oxidoreductase: An alternative enzyme for an alternative lifestyle. *Trends Parasitol* 23:305–310.
6. Hopkins AL (2008) Network pharmacology: The next paradigm in drug discovery. *Nat Chem Biol* 4:682–690.
7. Fisher N, Warman AJ, Ward SA, Biagini GA (2009) Chapter 17 Type II NADH: Quinone oxidoreductases *of Plasmodium falciparum* and *Mycobacterium tuberculosis* kinetic and high-throughput assays. *Methods Enzymol* 456:303–320.
8. Durant JL, Leland BA, Henry DR, Nourse JG (2002) Reoptimization of MDL keys for use in drug discovery. *J Chem Inf Comput Sci* 42:1273–1280.
9. Willett P (2006) Similarity-based virtual screening using 2D fingerprints. *Drug Discov Today* 11:1046–1053.
10. Geppert H, Vogt M, Bajorath J (2010) Current trends in ligand-based virtual screening: Molecular representations, data mining methods, new application areas, and performance evaluation. *J Chem Inf Model* 50:205–216.
11. Liu K, Feng J, Young SS (2005) PowerMV: A software environment for molecular viewing, descriptor generation, data analysis and hit evaluation. *J Chem Inf Model* 45:515–522.
12. Lipinski CA (2000) Drug-like properties and the causes of poor solubility and poor permeability. *J Pharmacol Toxicol Methods* 44:235–249.
13. Yeates CL, et al. (2008) Synthesis and structure-activity relationships of 4-pyridones as potential antimalarials. *J Med Chem* 51:2845–2852.
14. Cheng Y, Prusoff WH (1973) Relationship between the inhibition constant (K1) and the concentration of inhibitor which causes 50 per cent inhibition (I50) of an enzymatic reaction. *Biochem Pharmacol* 22:3099–3108.
15. Biagini GA, Viriyavejakul P, O'neill PM, Bray PG, Ward SA (2006) Functional characterization and target validation of alternative complex I of *Plasmodium falciparum* mitochondria. *Antimicrob Agents Chemother* 50:1841–1851.
16. Biagini GA, et al. (2008) Acridinediones: Selective and potent inhibitors of the malaria parasite mitochondrial bc1 complex. *Mol Pharmacol* 73:1347–1355.
17. Seymour KK, Yeo AE, Rieckmann KH, Christopherson RI (1997) dCTP levels are maintained in *Plasmodium falciparum* subjected to pyrimidine deficiency or excess. *Ann Trop Med Parasitol* 91:603–609.
18. Dembele L, et al. (2011) Towards an in vitro model of *Plasmodium* hypnozoites suitable for drug discovery. *PLoS ONE* 6:e18162.
19. Peters W, Robinson BL (1999) *Malaria* (Academic, San Diego).
20. Barton V, Fisher N, Biagini GA, Ward SA, O'Neill PM (2010) Inhibiting *Plasmodium* cytochrome bc1: A complex issue. *Curr Opin Chem Biol* 14:440–446.
21. Bray PG, Mungthin M, Ridley RG, Ward SA (1998) Access to hematin: The basis of chloroquine resistance. *Mol Pharmacol* 54:170–179.
22. Suswam E, Kyle D, Lang-Unnasch N (2001) *Plasmodium falciparum*: The effects of atovaquone resistance on respiration. *Exp Parasitol* 98:180–187.
23. Trager W, Jensen JB (1976) Human malaria parasites in continuous culture. *Science* 193:673–675.
24. Smilkstein M, Sriwilaijaroen N, Kelly JX, Wilairat P, Riscoe M (2004) Simple and inexpensive fluorescence-based technique for high-throughput antimalarial drug screening. *Antimicrob Agents Chemother* 48:1803–1806.
25. Delves M, et al. (2012) The activities of current antimalarial drugs on the life cycle stages of *Plasmodium*: A comparative study with human and rodent parasites. *PLoS Med* 9:e1001169.
26. Solmaz SR, Hunte C (2008) Structure of complex III with bound cytochrome c in reduced state and definition of a minimal core interface for electron transfer. *J Biol Chem* 283:17542–17549.
27. Rabinowitz JD, Kimball E (2007) Acidic acetonitrile for cellular metabolome extraction from *Escherichia coli*. *Anal Chem* 79:6167–6173.
28. O'Neill PM, et al. (2009) Candidate selection and preclinical evaluation of N-tert-butyl isoquine (GSK369796), an affordable and effective 4-aminoquinoline antimalarial for the 21st century. *J Med Chem* 52:1408–1415.